Atmospheric Chemistry of HFE-7100 ($C_4F_9OCH_3$): Reaction with OH Radicals, UV Spectra and Kinetic Data for $C_4F_9OCH_2\cdot$ and $C_4F_9OCH_2O_2\cdot$ Radicals, and the Atmospheric Fate of $C_4F_9OCH_2O\cdot$ Radicals

T. J. Wallington* and W. F. Schneider

Ford Research Laboratory, SRL-3083, Ford Motor Company, Dearborn, P.O. Box 2053, Michigan 48121-2053

J. Sehested,* M. Bilde, J. Platz, O. J. Nielsen,* and L. K. Christensen

Atmospheric Chemistry, Building 313, Plant Biology and Biogeochemistry Department, Risø National Laboratory, DK-4000 Roskilde, Denmark

M. J. Molina, L. T. Molina, and P. W. Wooldridge

Department of Earth, Atmospheric, and Planetary Science, 54-1820, Massachusetts Institute of Technology, Cambridge, Massachusetts 02139

Received: April 18, 1997; In Final Form: July 9, 1997[⊗]

Relative rate techniques were used to estimate k(OH+HFE-7100) $\approx 1.2 \times 10^{-14}$ cm^3 molecule^{-1} s^{-1} at 295 K leading to an estimate of ≈5 years for the atmospheric lifetime of HFE-7100 (HFE = hydrofluoroether). Pulse radiolysis transient UV absorption spectroscopy was used to study the ultraviolet absorption spectra and kinetics of $C_4F_9OCH_2$ and $C_4F_9OCH_2O_2$ radicals at 296 K. At 300 nm $\sigma(C_4F_9OCH_2) = (5.80 \pm 0.76) \times 10^{-19}$ and at 250 nm $\sigma(C_4F_9OCH_2O_2) = (2.24 \pm 0.24) \times 10^{-18}$ cm^2 molecule^{-1}. Both UV spectra showed two absorption maxima, one below 230 nm and one at 290 nm. Rate constants for the self-reactions of $C_4F_9OCH_2$ and $C_4F_9OCH_2O_2$ radicals, the reaction of $C_4F_9OCH_2$ radicals with O_2, and the reactions of $C_4F_9OCH_2O_2$ radicals with NO and NO_2 were $(3.5 \pm 0.8) \times 10^{-11}$, $(1.35 \pm 0.17) \times 10^{-11}$ (uncorrected for possible secondary chemistry), $(2.5 \pm 0.5) \times 10^{-12}$, $(8.5 \pm 2.5) \times 10^{-12}$, and $(8.8 \pm 1.8) \times 10^{-12}$ cm^3 molecule^{-1} s^{-1}, respectively. Using a pulse radiolysis method we measured k(F+HFE-7100) $= (1.6 \pm 0.6) \times 10^{-11}$ cm^3 molecule^{-1} s^{-1}. Using a Fourier transform infrared spectroscopic technique rate, constants for the reaction of F and Cl atoms with HFE-7100 and Cl atoms with $C_4F_9OC(O)H$ were determined to be $(1.3 \pm 0.3) \times 10^{-11}$, $(9.7 \pm 1.4) \times 10^{-14}$, and $(1.6 \pm 0.7) \times 10^{-14}$ cm^3 molecule^{-1} s^{-1}, respectively. Finally, it was determined that the sole atmospheric fate of $C_4F_9OCH_2O\cdot$ radicals is reaction with O_2 to give $C_4F_9OC(O)H$ (perfluorobutyl formate). The results are discussed with respect to the atmospheric chemistry of HFE-7100.

1. Introduction

Recognition of the adverse effect of chlorofluorocarbon (CFC) release into the atmosphere[1,2] has led to an international effort to replace CFCs with environmentally acceptable alternatives. Hydrofluoroethers (HFEs) are a class of fluid compounds which have been developed to replace CFCs in applications such as the cleaning of electronic equipment, heat transfer agents in refrigeration systems, and carrier fluids for lubricant deposition.[3] HFE-7100 ($C_4F_9OCH_3$) is one of the first HFEs to be used commercially. HFE-7100 is a volatile liquid with a vapor pressure of 210 Torr at 25 °C[3] and will be released into the atmosphere during its use. Prior to its large-scale industrial use an assessment of the atmospheric chemistry, and hence environmental impact, of HFE-7100 is needed.

The atmospheric oxidation of HFE-7100 will be initiated by reaction with OH radicals. The alkyl radical produced in reaction 1 will rapidly add O_2 to give a peroxy radical.

$$C_4F_9OCH_3 + OH \rightarrow C_4F_9OCH_2 + H_2O \quad (1)$$

$$C_4F_9OCH_2 + O_2 + M \rightarrow C_4F_9OCH_2O_2 + M \quad (2)$$

By analogy to other peroxy radicals,[4] $C_4F_9OCH_2O_2$ radicals will react with NO, NO_2, HO_2, and other peroxy radicals in the atmosphere.

$$C_4F_9OCH_2O_2 + NO \rightarrow C_4F_9OCH_2O + NO_2 \quad (3a)$$

$$C_4F_9OCH_2O_2 + NO + M \rightarrow C_4F_9OCH_2ONO_2 + M \quad (3b)$$

$$C_4F_9OCH_2O_2 + NO_2 + M \rightarrow C_4F_9OCH_2O_2NO_2 + M \quad (4)$$

$$C_4F_9OCH_2O_2 + HO_2 \rightarrow \text{products} \quad (5)$$

$$C_4F_9OCH_2O_2 + R'O_2 \rightarrow \text{products} \quad (6)$$

Experiments have been performed in our laboratories to elucidate the atmospheric chemistry of HFE-7100. A relative rate approach was used at the Massachusetts Institute of Technology (MIT) to measure the kinetics of the reaction of OH radicals with HFE-7100 and hence to provide an assessment of its atmospheric lifetime. A pulse radiolysis time-resolved UV−vis spectroscopic technique was used at Risø to obtain the UV absorption spectra of $C_4F_9OCH_2$ and $C_4F_9OCH_2O_2$ radicals and to study the kinetics of reactions 2−4 and 6. In the case of reaction 6 we studied the self-reaction of the peroxy radical ($R'O_2 = C_4F_9OCH_2O_2$). The fate of the alkoxy radical $C_4F_9OCH_2O$ produced in reaction 3a was determined using a Fourier transform infrared (FTIR) spectrometer coupled to a smog chamber at Ford Motor Company. To aid in the product identification, ab initio calculations were used at Ford Motor

[⊗] Abstract published in *Advance ACS Abstracts,* October 1, 1997.

S1089-5639(97)01353-4 CCC: $14.00

Company to provide insight into the IR spectrum of the formate C_4F_9OCHO. The results are reported herein and discussed with respect to the environmental impact of HFE-7100.

2. Experimental Section

The three experimental systems used are described in detail elsewhere.[5,6,7] All samples of HFE-7100 used in this work were supplied by the 3M Company. Experiments performed at MIT employed a sample of HFE-7100, which was a mixture of 95% *n*-$C_4F_9OCH_3$ ($CF_3CF_2CF_2CF_2OCH_3$) and 5% *i*-$C_4F_9OCH_3$ ($(CF_3)_2CFCF_2OCH_3$). Experiments at Risø were conducted using a commercial sample of HFE-7100, which was a mixture of 35% *n*-$C_4F_9OCH_3$ and 65% *i*-$C_4F_9OCH_3$. During the experiments at Ford Motor Company, samples of pure *i*-$C_4F_9OCH_3$ and *n*-$C_4F_9OCH_3$ became available and were used. In light of the structural similarities between the two HFE-7100 isomers and their corresponding alkyl and alkyl peroxy radicals, it is assumed that the spectroscopic and kinetic results obtained at MIT and Risø using the mixture of isomers are representative of the individual pure isomers. Evidence supporting this assumption was obtained from the work at Ford and is discussed in sections 3.10 and 3.11. The uncertainties reported in this paper are two standard deviations unless otherwise stated. Standard error propagation methods were used to calculate combined uncertainties.

2.1. FTIR−Photolysis System at MIT. An approximate value for the rate of OH + HFE-7100 reaction was obtained by monitoring the disappearance rate of HFE-7100 relative to that of a reference compound (CH_4 or CH_3Cl) in the presence of OH radicals at 295 K. The decay of the sample was measured using infrared spectroscopy.[5] The concentration of HFE-7100 was monitored by spectral subtraction; within the experimental error all the bands decreased at the same rate, indicating that the OH reaction rate constant is practically the same for the *n*- and *i*-isomers. OH radicals were generated by photolysis of ozone at 254 nm in the presence of water vapor:

$$O_3 + h\nu \rightarrow O(^1D) + O_2 \quad (7)$$

$$O(^1D) + H_2O \rightarrow 2\ OH \quad (8)$$

The long-path absorption cell, made of Pyrex glass, had a volume of 7.6 L and a base length of 60 cm, which was adjusted to give a total of 24 passes and an optical path of 14.4 m. The concentrations of the reactants and products were monitored with an FTIR spectrometer (Nicolet 20SX). The photolysis lamp (Ace Hanovia 450 W medium-pressure mercury lamp) was placed inside the absorption cell, enveloped in a Vycor tube, which transmits 254 nm radiation but absorbs the 185 nm Hg line. No decay of the HFE-7100 sample was observed in the absence of ozone.

The organic reactants were mixed with helium in a 3 L glass reservoir to yield mole fractions of ∼1%. Ozone was prepared by first trapping the effluent from an ozonizer in cold silica gel and then desorbing the sample into a 3 L glass reservoir and subsequently mixing it with helium. The experiments were performed at room temperature in ∼200 Torr helium as a buffer gas, in the presence of ∼1 Torr ozone.

2.2. Pulse Radiolysis System at Risø National Laboratory. A pulse radiolysis transient UV absorption apparatus[6] was used to study the UV absorption spectra and kinetics of $C_4F_9OCH_2$ and $C_4F_9OCH_2O_2$ radicals. Radicals were generated by radiolysis of gas mixtures in a 1 L stainless steel reactor by a 30 ns pulse of 2 MeV electrons from a Febetron 705B field emission accelerator. The radiolysis dose, referred to herein as a fraction of maximum dose, was varied by insertion of stainless steel attenuators between the accelerator and the chemical reactor. The analyzing light was provided by a pulsed Xenon arc lamp, reflected in the reaction cell by internal White type optics, dispersed using a 1 m McPherson monochromator (operated at a spectral resolution of 0.8 nm), and detected by a photomultiplier. All transients were results of single pulse experiments with no signal averaging.

SF_6 was used as the diluent gas. Radiolysis of SF_6 produces fluorine atoms:

$$SF_6 + 2\ \text{MeV}\ e^- \rightarrow F + \text{products} \quad (9)$$

SF_6 was always present in great excess to minimize the relative importance of direct radiolysis of other compounds in the gas mixtures. The fluorine atom yield was determined by measuring the yield of CH_3O_2 radicals following radiolysis of mixtures of 10 mbar CH_4, 40 mbar O_2, and 950 mbar SF_6:

$$F + CH_4 \rightarrow CH_3 + HF \quad (10)$$

$$CH_3 + O_2 + M \rightarrow CH_3O_2 + M \quad (11)$$

CH_3O_2 radicals were monitored using their absorption at 260 nm. On the basis of $\sigma_{260nm}(CH_3O_2) = 3.18 \times 10^{-18}$ cm^2 molecule^{-1} [9] the F atom yield at full radiolysis dose and 1000 mbar SF_6 was determined to be $(3.18 \pm 0.32) \times 10^{15}$ cm^{-3}.[8] The quoted uncertainty reflects both statistical uncertainties associated with the calibration procedure and a 10% uncertainty in $\sigma(CH_3O_2)$.[9]

Reagents used were 0−27 mbar O_2 (ultrahigh purity), 950−1000 mbar SF_6,(99.9%), 0−19 mbar $C_4F_9OCH_3$ (>99%), 0−0.95 mbar NO (>99.8%), 0−1.3 mbar NO_2 (>98%), and 0−10 mbar CH_4, (>99%). All were used as received. The HFC-7100 sample was repeatedly degassed by freeze−pump−thaw cycles before use.

2.3. FTIR−Smog Chamber System at Ford Motor Company. All experiments were performed in a 140 L Pyrex reactor interfaced to a Mattson Sirus 100 FTIR spectrometer.[7] The reactor was surrounded by 22 fluorescent black lamps (GE F15T8-BL) which were used to photochemically initiate the experiments. The oxidation of HFE-7100 was initiated by reaction with Cl atoms, which were generated by the photolysis of molecular chlorine in O_2/N_2 diluent at 700 Torr total pressure at 295 ± 2 K,

$$Cl_2 + h\nu \rightarrow 2Cl \quad (12)$$

$$Cl + C_4F_9OCH_3 \rightarrow C_4F_9OCH_2 + HCl \quad (13)$$

$$C_4F_9OCH_2 + O_2 + M \rightarrow C_4F_9OCH_2O_2 + M \quad (2)$$

The loss of HFE-7100 and the formation of products were monitored by FTIR using an infrared path length of 27 m and a resolution of 0.25 cm^{-1}. Infrared spectra were derived from 32 coadded interferograms.

Two sets of experiments were performed. First, relative rate techniques were used to determine the rate constant for the reaction of Cl and F atoms with HFE-7100. Second, the products of the atmospheric oxidation of HFE-7100 were investigated by irradiating HFE-7100/$Cl_2/O_2/N_2$ mixtures with, and without, added NO.

Initial concentrations of the gas mixtures for the relative rate experiments were 5 mTorr of HFE-7100, 15−40 mTorr of the reference organic, and either 0.1−0.2 Torr of Cl_2, or 0.5−1.0 Torr of F_2, in 700 Torr of either N_2 or air diluent. In the study of the oxidation of HFE-7100, reaction mixtures consisted of

TABLE 1: OH Reaction Rates with HFE-7100 Sample

[HFE-7100] (mTorr)	ref (mTorr)	water (Torr)	photolysis time (min)	fraction of sample remaining after reaction with OH	fraction of reference remaining after reaction with OH	$k_1/k_{OH+REFERENCE}$
23	CH_4: 29	1.6	2.5	0.83	0.89	1.6
28	CH_4: 37	1.1	3.0	0.70	0.90	3.3
23	CH_3Cl: 25	1.6	2.5	0.83	0.58	0.35
29	CH_3Cl: 53	1.6	3.0	0.81	0.52	0.32

5−15 mTorr of HFE-7100, 0.1−0.2 Torr of Cl_2, 0−16 mTorr of NO, and 40−700 Torr of O_2 at a total pressure of 700 Torr in N_2 diluent. All experiments were performed at 295 K.

Computational Details. Hartree−Fock and second-order Møller−Plesset (MP2) calculations were performed using the GAMESS[10] and ACES II[11] programs, respectively. Molecular geometries, vibrational frequencies, and intensities were calculated analytically at the Hartree−Fock level with Pople's 6-31G(d,p) basis.[12] The geometries were further refined at MP2 level[13,14] using the 6-31G(d,p), and final energies obtained using the TZ2P[11] basis with core electrons frozen.

3. Results and Discussion

3.1. Reaction of OH with HFE-7100 Investigated at MIT. HFE-7100 reacted several times faster with OH than methane and several times slower than methyl chloride. The results of the kinetics runs are presented in Table 1. Using CH_3Cl as a reference, we estimate the rate constant for the OH + HFE-7100 reaction to be $\approx 1.2 \times 10^{-14}$ cm^3 molecule^{-1} s^{-1}, based on a rate constant value for CH_3Cl + OH of 3.6×10^{-14} cm^3 molecule^{-1} s^{-1}.[15] Within experimental error the result using CH_4 as a reference is the same, but the uncertainty is larger, since only about 10% of the CH_4 reacted with OH. Furthermore, assuming an atmospheric lifetime for methane of 9 years[16] and a rate constant for the CH_4 + OH reaction of 6.3×10^{-15} cm^3 molecule^{-1} s^{-1} leads to an HFE-7100 atmospheric lifetime against reaction with OH of ≈5 years.

3.2. UV Absorption Spectrum of the $C_4F_9OCH_2$ Radical. Following the pulse radiolysis of mixtures of 5 mbar of HFE-7100 and 995 mbar of SF_6, a rapid (complete within 1−2 μs) increase in absorption at 300 nm was observed, followed by a slower decay. Figure 1A shows a typical absorption transient. No absorption was observed when either 5 mbar of HFE-7100 or 995 mbar of SF_6 were subject to pulse radiolysis separately. We ascribe the absorption in Figure 1A to the formation of $C_4F_9OCH_2$ radicals via reaction 14 and their subsequent loss via self-reaction 15.

$$F + C_4F_9OCH_3 \rightarrow C_4F_9OCH_2 + HF \qquad (14)$$

We assume that F atoms react with HFE-7100 exclusively via H-atom abstraction. To determine the absorption cross section of the $C_4F_9OCH_2$ radical at 300 nm, the maximum transient absorbance was recorded at various radiolysis doses. Figure 2 (circles) shows a plot of the observed maximum absorbance as a function of the radiolysis dose (and hence initial radical concentration). The absorbance is proportional to the dose up to 42% of full dose suggesting that unwanted radical−radical reactions, such as reactions 15 and 16, are unimportant in this range.

$$C_4F_9OCH_2 + C_4F_9OCH_2 + M \rightarrow \text{products} \qquad (15)$$

$$F + C_4F_9OCH_2 \rightarrow \text{products} \qquad (16)$$

Linear least-squares regression of the low-dose data in Figure 2 gives a slope of $(9.56 \pm 0.80) \times 10^{-2}$. Combining this result with the calibrated fluorine atom yield of $(3.18 \pm 0.32) \times 10^{15}$ cm^{-3} at full dose and 1000 mbar of SF_6 and the optical path length of 120 cm gives $\sigma_{300nm}(C_4F_9OCH_2) = (5.80 \pm 0.76) \times 10^{-19}$ cm^2 molecule^{-1}. The UV absorption spectrum in the range 220−320 nm was mapped out by comparing the absorption at a given wavelength to that at 300 nm and scaling using $\sigma_{300nm}(C_4F_9OCH_2) = 5.8 \times 10^{-19}$ cm^2 molecule^{-1}. The results are listed in Table 2 and plotted in Figure 3 together with the spectrum of CH_3OCH_2 radicals. As seen from Figure 3, the spectra of these radicals are similar in shape with two absorption maxima, one below 225 nm and one at 280−300 nm. Replacement of the CH_3 group by the electron-withdrawing C_4F_9 group on the $-OCH_2^{\bullet}$ chromophore decreases the absorption cross section by a factor of 2−4.

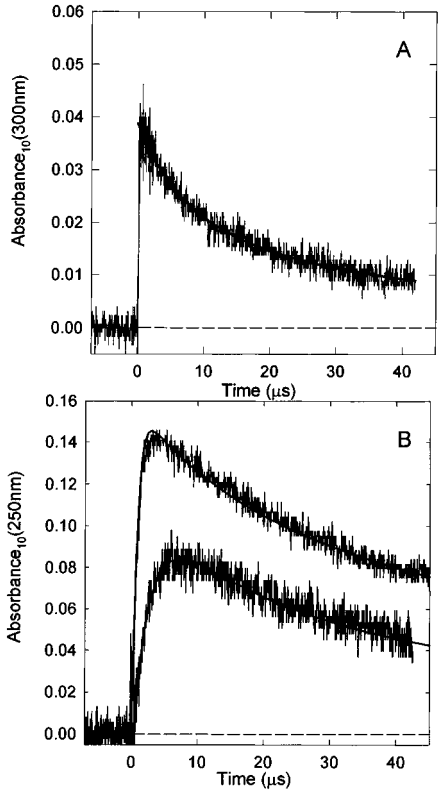

Figure 1. Transient absorption following radiolysis of mixtures of (A) 5 mbar $C_4F_9OCH_3$ and 995 mbar SF_6, 42% of maximum dose, optical path length 120 cm and (B) 5 mbar HFE-7100, 27 mbar O_2 (upper curve) or 6.1 mbar of O_2 (lower curve) and SF_6 added to 1000 mbar total pressure, 42% of maximum dose, and optical path length 120 and 80 cm, respectively. The absorbance were recorded at (A) 300 and (B) 250 nm. Absorption is ascribed to (A) $C_4F_9OCH_2$ radicals and (B) $C_4F_9OCH_2O_2$ radicals. The smooth line in (A) is a second-order decay fit to the data. The smooth lines in (B) are simulations using a chemical model; see text for details.

3.3. Kinetics of the Self-Reaction of $C_4F_9OCH_2$ Radicals. The rate constant for the self-reaction of $C_4F_9OCH_2$ radicals was determined by monitoring the rate of decay of the absorption at 300 nm following pulse radiolysis of mixtures of 5 mbar of HFE-7100 and 995 mbar of SF_6. The half-lives of the decays were derived from a fit to the data using a second-order expression: $A(t) = A_{inf} + (A_0 - A_{inf})/(1 + k'(A_0 - A_{inf})t)$, where $A(t)$ is the time dependent absorbance and A_0 and A_{inf}

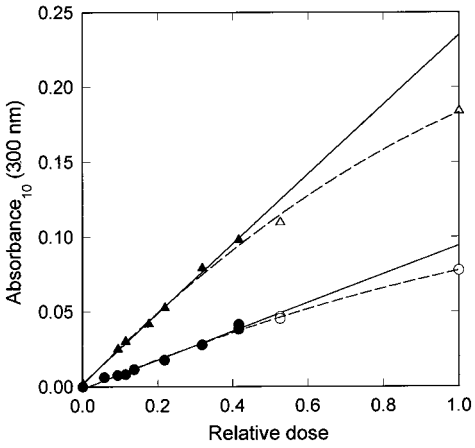

Figure 2. Maximum transient absorptions observed following radiolysis of mixtures of 5 mbar $C_4F_9OCH_3$, and 995 mbar SF_6 (circles); 5 mbar $C_4F_9OCH_3$, 27 mbar O_2, and 968 mbar SF_6 (triangles). UV path lengths (l) were 120 and 80 cm, respectively, and the transients were recorded at 300 and 250 nm, respectively. Solid lines are least-squares fits to the low-dose data (filled symbols), and the dashed lines are polynomial fit to the experimental data to help the visual inspection of the data.

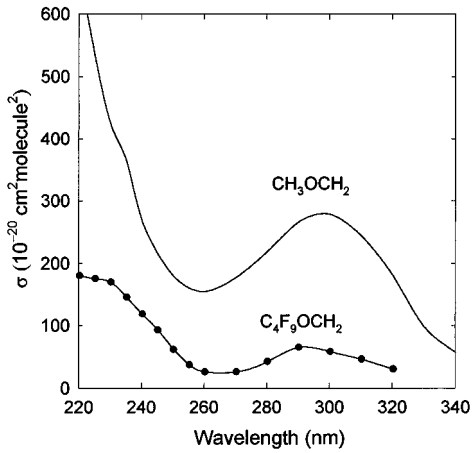

Figure 3. Spectra of $C_4F_9OCH_2$ (circles) and CH_3OCH_2 radicals.

TABLE 2: Measured UV Absorption Cross Sections

wavelength (nm)	$\sigma(C_4F_9OCH_2) \times 10^{20}$ (cm^2 molecule^{-1})	$\sigma(C_4F_9OCH_2O_2) \times 10^{20}$ (cm^2 molecule^{-1})
220	181	512
225	176	489
230	170	455
235	145	404
240	128	341
245	93	280
250	62	224
255	37	178
260	26	136
270	26	85
280	42	63
290	65	67
300	58	61
310	46	44
320	30	33

are the absorbances at $t = 0$, and at $t = \infty$, respectively, and $k' = 2k_{15}\sigma_{300nm}(C_4F_9OCH_2)l/\ln 10$. k_{15} is the rate constant for reaction 15, l is the optical path length, 120 cm, and $\sigma_{C_4F_9OCH_2}$(300 nm) = $(5.80 \pm 0.76) \times 10^{-19}$ cm^2 molecule^{-1}. The decays were always well described by the second-order expression above. An example of a fit is shown in Figure 1A. The filled circles in Figure 4A show the reciprocal of the decay half-lives at various doses versus the maximum transient absorbance. A linear regression analysis gives a slope of $(2.33 \pm 0.40) \times 10^6$ s^{-1}. This slope equals $k_{15}[2(2.303)]/(l\,\sigma_{300nm}(C_4F_9OCH_2))$. Hence, $k_{15} = (3.5 \pm 0.8) \times 10^{-11}$ cm^3 molecule^{-1} s^{-1}. The quoted uncertainty includes uncertainties in both the slope of the line in Figure 4A and in $\sigma_{300nm}(C_4F_9OCH_2)$.

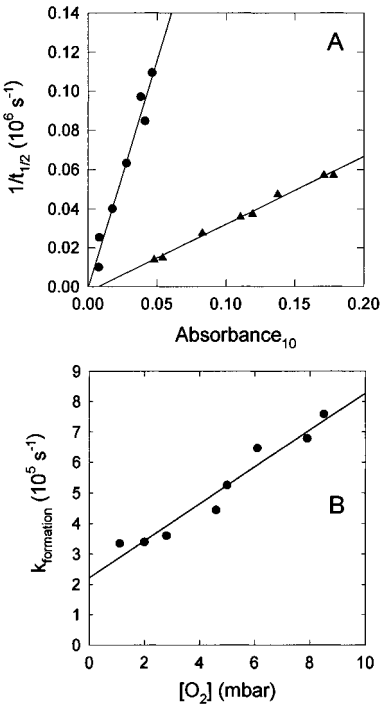

Figure 4. (A) The reciprocal half-lives for the self-reaction of $C_4F_9OCH_2$ radicals (circles) versus the maximum transient absorbance at 300 nm. The reciprocal half-lives of the decay of $C_4F_9OCH_2O_2$ radicals due to self-reaction (triangles) versus the maximum transient absorbance at 250 nm. (B) The pseudo-first-order formation rate constant of $C_4F_9OCH_2O_2$ radicals plotted as a function of the initial oxygen pressure. The lines are linear regressions.

3.4. Kinetics of the F + $C_4F_9OCH_3$ Reaction. The rate constant ratio k_{14}/k_{17} was determined from the maximum transient absorption at 230 nm following pulse radiolysis of mixtures of 0−18.3 mbar of $C_4F_9OCH_3$, 50 mbar of CF_3CCl_2H, and 1000 mbar SF_6. Reactions 14 and 17 compete for the available F atoms.

$$F + C_4F_9OCH_3 \rightarrow C_4F_9OCH_2 + HF \qquad (14)$$

$$F + CF_3CCl_2H \rightarrow CF_3CCl_2 + HF \qquad (17)$$

The alkyl radical CF_3CCl_2 formed by reaction of F atoms with CF_3CCl_2H (HCFC-123) absorbs strongly at 230 nm ($\sigma_{CF_3CCl_2} = 9.7 \times 10^{-18}$ cm^2 molecule^{-18}). In contrast, absorption by the $C_4F_9OCH_2$ radical is significantly weaker ($\sigma_{C_4F_9OCH_2} = 1.7 \times 10^{-18}$ cm^2 molecule^{-1}, see Table 2). Figure 5 shows the observed variation of the maximum transient absorbance at 230 nm as a function of the concentration ratio $[C_4F_9OCH_3]/[CF_3CCl_2H]$. As shown in Figure 5, the maximum transient absorption decreases with increasing $C_4F_9OCH_3$ concentration because a greater fraction of the F atoms react with $C_4F_9OCH_3$.

The data in Figure 5 can be fitted with a three parameter expression:

$$A_{max} = \frac{A_{CF_3CCl_2} + A_{C_4F_9OCH_2}\left[\frac{k_{14}}{k_{17}}\right]\left\{\frac{[C_4F_9OCH_3]}{[CF_3CCl_2H]}\right\}}{1 + \left[\frac{k_{14}}{k_{17}}\right]\left\{\frac{[C_4F_9OCH_3]}{[CF_3CCl_2H]}\right\}}$$

where A_{max}, $A_{CF_3CCl_2}$, and $A_{C_4F_9OCH_2}$ are the observed maximum

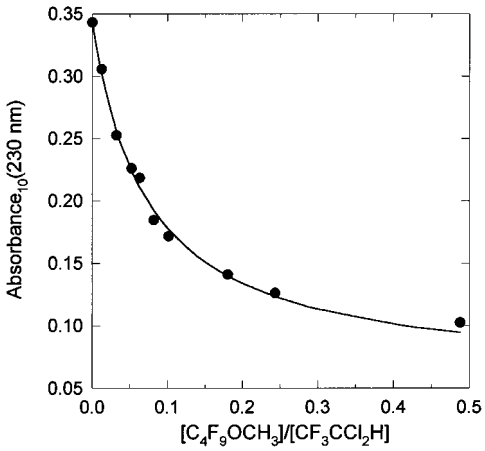

Figure 5. The maximum transient absorbance at 230 nm plotted as function of $[C_4F_9OCH_3]/[CF_3CCl_2H]$. The smooth line is a fit to the data; see text for details.

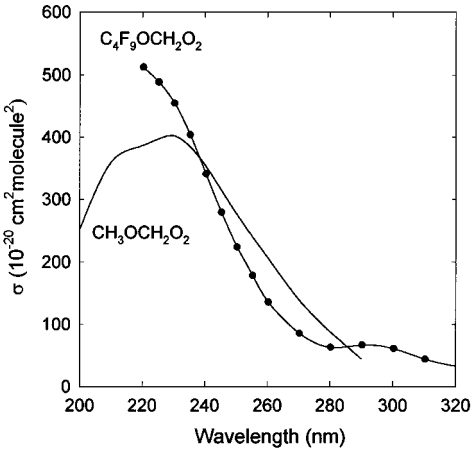

Figure 6. Spectra of $C_4F_9OCH_2O_2$ (circles) and $CH_3OCH_2O_2$ radicals.

absorbance for the mixture of radicals, the maximum absorbance expected if all F atoms react with CF_3CCl_2H, and the maximum absorbance expected if all F atoms react with $C_4F_9OCH_3$, respectively. $A_{CF_3CCl_2}$, $A_{C_4F_9OCH_2}$, and k_{14}/k_{17} were simultaneously varied, and the best fit was achieved with $A_{CF_3CCl_2} = 0.34 \pm 0.01$, $A_{C_4F_9OCH_2} = 0.06 \pm 0.01$, and $k_{14}/k_{17} = (13.7 \pm 1.6)$. The results for $A_{CF_3CCl_2}$ and $A_{C_4F_9OCH_2}$ are consistent with those expected on the basis of the absorption cross sections of the CF_3CCl_2 and $C_4F_9OCH_2$ radicals given above. Using $k_{17} = (1.2 \pm 0.4) \times 10^{-12}$ cm^3 molecule^{-1} s^{-1} [17] gives $k_{14} = (1.6 \pm 0.6) \times 10^{-11}$ cm^3 molecule^{-1} s^{-1}. This result is in good agreement with the value of $(1.3 \pm 0.3) \times 10^{-11}$ cm^3 molecule^{-1} s^{-1} determined using the FTIR technique as described in section 3.10.

3.5. UV Absorption Spectrum of the $C_4F_9OCH_2O_2$ Radical. To study the UV spectrum of the peroxy radical $C_4F_9OCH_2O_2$, mixtures of 5 mbar of $C_4F_9OCH_3$, 27 mbar of O_2, and 968 mbar SF_6 were subject to pulse radiolysis and the resulting transient absorbance was monitored over the wavelength range 220−320 nm. Typical experimental absorption transients recorded at a monitoring wavelength of 250 nm are shown in Figure 1B. The maximum absorption observed at 250 nm following the radiolysis of SF_6/HFE-7100/O_2 mixtures was 3−4 times that observed following radiolysis of SF_6/HFE-7100 mixtures. We attribute the absorption observed using SF_6/HFE-7100/O_2 mixtures to the formation of $C_4F_9OCH_2O_2$ radicals by the consecutive set of reactions 9, 14, and 2.

To derive the UV absorption spectrum of the $C_4F_9OCH_2O_2$ radical, we need to work under conditions where unwanted secondary radical−radical reactions, such as reactions 15, 16, and 18−20, are avoided or minimized.

$$C_4F_9OCH_2O_2 + C_4F_9OCH_2O_2 \rightarrow \text{products} \quad (18)$$

$$C_4F_9OCH_2O_2 + C_4F_9OCH_2 \rightarrow \text{products} \quad (19)$$

$$C_4F_9OCH_2O_2 + F \rightarrow \text{products} \quad (20)$$

In addition, the reaction of F atoms with O_2 needs to be minimized:

$$F + O_2 + M \rightarrow FO_2 + M \quad (21)$$

To minimize the amount of F atoms consumed by reaction 21 the oxygen concentration should be low. However, a low oxygen concentration will increase the importance of reactions 15, 16, and 19. Clearly, a compromise is needed. An initial O_2 concentration of 27 mbar was chosen. Under these experimental conditions, 6.0% of the F atoms are converted into FO_2 ($k_{21} = 1.9 \times 10^{-13}$ [18] and $k_{14} = 1.6 \times 10^{-11}$ cm^3 molecule^{-1} s^{-1}). Absolute values for the absorption cross sections (in units of 10^{-20} cm^2 molecule^{-1}) of FO_2 at different wavelengths are[18] $\sigma_{225nm} = 755$, $\sigma_{230nm} = 508$, $\sigma_{235nm} = 341$, $\sigma_{240nm} = 180$, $\sigma_{245nm} = 153$, and $\sigma_{254nm} = 69$, and these values can be used to correct for the absorbance caused by FO_2 radicals.

There are no literature data concerning the kinetics of reactions 16, 19, and 20, so we cannot calculate their importance. To check for these unwanted radical−radical reactions the transient absorption at 250 nm was measured in experiments using $[C_4F_9OCH_3] = 5$ mbar, $[O_2] = 27$ mbar, and $[SF_6] = 968$ mbar with the radiolysis dose (and hence initial radical concentration) varied over an order of magnitude. The UV path length was 80 cm. The triangles in Figure 2 show the observed maximum transient absorption as a function of the dose. As seen from Figure 2, the absorption is linear with radiolysis dose up to 42% of maximum dose. This linearity indicates that at low radiolysis doses unwanted secondary radical−radical reactions are not important. The solid line drawn through the data in Figure 2 is a linear least-squares fit to the low-dose data which gives a slope of 0.2328 ± 0.0095. From this and three additional pieces of information, (i) the F atom yield of $(3.18 \pm 0.32) \times 10^{15}$ cm^{-3} (full dose and $[SF_6] = 1000$ mbar), (ii) the conversion of F atoms into $C_4F_9OCH_2O_2$ (94%) and FO_2 (6%), and (iii) the absorption cross section for FO_2 at 250 nm ($\sigma = 1.26 \times 10^{-18}$ cm^2 molecule^{-1} [19]), we derive $\sigma(C_4F_9OCH_2O_2)$ at 250 nm $= (2.24 \pm 0.24) \times 10^{-18}$ cm^2 molecule^{-1}. The quoted uncertainty reflects both two standard deviations from the linear least-squares fit to the low-dose data in Figure 2 and the uncertainty in the absolute calibration of the fluorine atom yield.

To map out the spectrum of the $C_4F_9OCH_2O_2$ radical, the maximum transient absorbance was measured over the range 220−310 nm, scaled to that at 250 nm, and placed on an absolute basis using $\sigma(250\text{ nm}) = 2.24 \times 10^{-18}$ cm^2 molecule^{-1}. A small correction (<11%) was applied to account for the formation of FO_2 using the formula: $\sigma_{corrected} = [(\sigma_{raw} - \sigma_{FO_2})0.06]/0.94$. The results are plotted in Figure 6 and listed in Table 2.

The spectrum of $CH_3OCH_2O_2$ radicals is shown in Figure 6 for comparison. As seen from the figure, the spectrum of $C_4F_9OCH_2O_2$ appears to be blue-shifted relative to that of $CH_3OCH_2O_2$. Interestingly, from a comparison of the spectra in Figures 3 and 6 it can be seen that the absorption maximum at 290 nm evident in the spectrum of $C_4F_9OCH_2$ radicals is preserved in the spectrum of the peroxy radical $C_4F_9OCH_2O_2$

radicals. In contrast, the absorption maximum at 290 nm evident in the spectrum of CH_3OCH_2 radicals does not appear to be preserved in the spectrum of the peroxy radical $CH_3OCH_2O_2$. The reason for this difference is unknown.

3.6. Association Reaction between O_2 and the $C_4F_9OCH_2$ Radical. The rate constant for the reaction between $C_4F_9OCH_2$ radicals and O_2 was measured by monitoring the rate of increase in absorption at 250 nm at short times (2−10 μs) following pulsed radiolysis (42% dose) of mixtures of 5 mbar of HFE-7100, 1.1−8.5 mbar of O_2, and 990 mbar of SF_6. As discussed above, the peroxy radical $C_4F_9OCH_2O_2$ absorbs strongly at 250 nm ($\sigma = 2.24 \times 10^{-18}$ cm^2 molecule^{-1}) and its formation can be monitored easily. The lower traces in Figure 1B are examples of traces used to measure k_2. The rise of absorption in Figure 1B contains information on the rate constant k_2. This information was extracted using two different methods. The first method was to fit a first-order rise expression to the increase in absorption. The expression used was: $A(t) = (A_0 - A_{inf})\cdot\exp(-k_{formation}t) + A_{inf}$, where $k_{formation}$ is the pseudo-first-order formation rate constant, $A(t)$ is the absorbance as function of time, A_0 is the maximum absorbance by $C_4F_9OCH_2$ radicals, and A_{inf} is the maximum absorbance by $C_4F_9OCH_2O_2$ radicals. $k_{formation}$, A_0, and A_{inf} were used as fit parameters. To account for the finite time taken for the formation of $C_4F_9OCH_2$ in the system, the fits were started 1 μs after the radiolysis pulse at which time conversion of F atoms into $C_4F_9OCH_2$ radicals is 86% complete. In Figure 4B the pseudo first-order-formation rate constants ($k_{formation}$) are plotted as function of [O_2]. Linear least squares gives $k_2 = (2.5 \pm 0.5) \times 10^{-12}$ cm^3 molecule^{-1} s^{-1}. There is a significant positive y-axis intercept in Figure 4B which, based upon our experience with such systems, we attribute to the influence of loss of $C_4F_9OCH_2$ radicals via their self-reaction. The second method used to derive k_2 was a detailed modeling approach using the Chemsimul program[20] with a chemical mechanism consisting of reactions 2, 14, 15, 18, and 21 with $k_{F+RH} = 1.6 \times 10^{-11}$, $k_{F+O_2} = 1.9 \times 10^{-13}$, $k_{R+O_2} = 2.5 \times 10^{-12}$, $k_{R+R} = 3.5 \times 10^{-11}$, $k_{RO_2+RO_2} = 1.35 \times 10^{-11}$ cm^3 molecule^{-1} s^{-1}, $\sigma_{250nm}(C_4F_9OCH_2O_2) = 224 \times 10^{-20}$, and $\sigma_{250nm}(C_4F_9OCH_2) = 62 \times 10^{-20}$ cm^2 molecule^{-1}. The results of such two simulations are shown as the smooth curves in Figure 1B. In all cases the observed transients were well described using $k_2 = (2.5 \pm 0.5) \times 10^{-12}$ cm^3 molecule^{-1} s^{-1}.

3.7. Kinetics of the Self-Reaction of $C_4F_9OCH_2O_2$ Radicals. Figure 1B shows typical transient absorptions obtained following the pulsed radiolysis of $C_4F_9OCH_3/SF_6/O_2$ mixtures. The decay of the absorption is due to the self-reaction of the $C_4F_9OCH_2O_2$ radical:

$$C_4F_9OCH_2O_2 + C_4F_9OCH_2O_2 \rightarrow \text{products} \qquad (18)$$

The rate constant of reaction 18 is defined by the equation $-d[C_4F_9OCH_2O_2]/dt = 2k_{18obs}[C_4F_9OCH_2O_2]^2$. The observed rate constant k_{18obs} for reaction 18 can be obtained from a plot of the reciprocal half-lives of the peroxy radical decay versus the maximum transient absorbance measured at 250 nm. The triangles in Figure 4A show such a plot. The absorbances are corrected for the absorption due to FO_2 = according to the formula $A = [A_{obs} - \sigma(FO_2)](80\text{ cm})(0.06)(3.08 \times 10^{15})$ (molecule cm^{-3})dose. The decay half-lives were derived from a fit to the transients using the second-order expression: $A(t) = A_{inf} + (A_0 - A_{inf})/(1 + k'(A_0 - A_{inf})t)$, where $A(t)$ is the time dependent absorbance and A_0 and A_{inf} are the absorbances at $t = 0$ and at $t = \infty$, respectively. $k' = k_{18}/\sigma_{C_4F_9OCH_2O_2}(250\text{ nm})/[(2.303)(2)]$ where k_{18} is the second-order rate constant for the self-reaction of the radicals. The decays were always well described by second-order kinetics. For these experiments the optical path length (l) was 80 cm, [$C_4F_9OCH_3$] = 5 mbar, [O_2] = 30 mbar, [SF_6] = 965 mbar, and the dose was varied between full and 21% of full dose.

A linear regression analysis of the data in Figure 4A gives a slope of $(3.47 \pm 0.25) \times 10^5$ s^{-1}which equals $k_{18obs}(2 \times 2.303)/(l\sigma_{C_4F_9OCH_2O_2}(250\text{ nm}))$ where k_{18obs} is the observed rate constant for reaction 18, l is the optical path length, 80 cm, and $\sigma_{C_4F_9OCH_2O_2}(250\text{ nm}) = (2.24 \pm 0.24) \times 10^{-18}$ cm^2 molecule^{-1}. Hence, $k_{18obs} = (1.35 \pm 0.17) \times 10^{-11}$ cm^3 molecule^{-1} s^{-1}. In addition to reaction 18, the decay of the $C_4F_9OCH_2O_2$ radical may also be influenced by reactions with other radicals, for example,

$$C_4F_9OCH_2O + O_2 \rightarrow HO_2 + C_4F_9OCHO \qquad (22)$$

$$HO_2 + C_4F_9OCH_2O_2 \rightarrow \text{products} \qquad (23)$$

$$C_4F_9OCH_2O_2 + C_4F_9OCH_2O \rightarrow \text{products} \qquad (24)$$

Since the rate constants for reactions 22−24 are unknown, we cannot correct for these reactions at the present time. Our reported value of k_{18obs} is the observed rate constant which describes the rate of decay of absorption at 250 nm in the present system. It is interesting to compare k_{18obs} with the rate constants for the self-reaction of other peroxy radicals. Consider the radicals CH_3O_2, $CH_3CH_2O_2$, $HOCH_2O_2$, $CH_3OCH_2O_2$, $CH_3C(O)CH_2O_2$, and $CH_3OC(O)OCH_2O_2$. The rate constants for the self-reactions are (in units of cm^3 molecule^{-1} s^{-1}) 3.7×10^{-13},[19] 7.0×10^{-14},[19] 7.0×10^{-12},[19] 2.7×10^{-12},[19] 8.3×10^{-12},[19] and 1.27×10^{-11} (observed only),[18] respectively. As noted previously[9,19] electron-withdrawing substituents increase the reactivity of peroxy radicals toward self-reaction.

3.8. Rate Constant for the Reaction $C_4F_9OCH_2O_2 + NO_2 + M \rightarrow C_4F_9OCH_2O_2NO_2 + M$. Following the radiolysis (42% dose) of mixtures of 970 mbar of SF_6, 5 mbar of $C_4F_9OCH_3$, 25 mbar of O_2, and 0.21−1.3 mbar of NO_2, a rapid (complete within 40 μs) decrease in absorption at 400 nm was observed. Figure 7A−C show typical absorption transients. We ascribe the decrease in absorption to loss of NO_2 via reaction with $C_4F_9OCH_2O_2$ radicals. The absorption transient from each experiment was fitted using the Chemsimul program[20] with a chemical mechanism consisting of the following reactions and rate constants (R = $C_4F_9OCH_2$): F + RH (1.6×10^{-11}), F + NO_2 (1.0×10^{-11}), R + NO_2 (1.0×10^{-11}), R + O_2 (2.5×10^{-12}), R + R (3.5×10^{-11}), RO_2 + RO_2 (1.35×10^{-11}), and RO + NO_2 (1×10^{-11}), with k_4 varied to give the best fit. As shown by the solid curves in Figure 7A−C, the experimental transients were best fit using $k_4 = 8.8 \times 10^{-12}$ cm^3 molecule^{-1} s^{-1}. To illustrate the sensitivity of the fit, the dotted curves in Figure 7C show the effect of varying k_4 by ±20%. We estimate that $k_4 = (8.8 \pm 1.8) \times 10^{-12}$ cm^3 molecule^{-1}s^{-1}. At 1000 mbar of SF_6 it is expected that k_4 is close to its high-pressure limit. The value of k_4 obtained here is similar to the high-pressure limiting rate constants for the reactions of other peroxy radicals with NO_2 which lie in the range $(5-10) \times 10^{-12}$ cm^3 molecule^{-1} s^{-1}.[19]

3.9. Rate Constant for the Reaction $C_4F_9OCH_2O_2 + NO \rightarrow$ Products. The rate constant for the reaction of NO with $C_4F_9OCH_2O_2$ was studied using the pulsed radiolysis setup. Following the radiolysis of $SF_6/C_4F_9OCH_3/O_2/NO$ mixtures, an increase in absorption at 400 nm was observed. Figure 7D shows a typical absorption transient. Experiments were performed using 42% of full dose, with mixtures of 5 mbar of HFE-7100, 25 mbar of O_2, 954 mbar of SF_6, and 0.31−0.95 mbar of NO. The increase in absorption is ascribed to NO_2 formation via reaction 3a. For each concentration of NO the

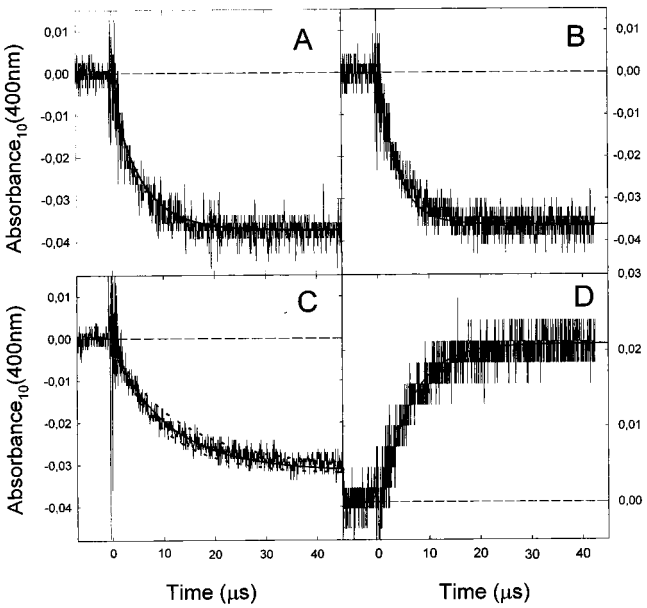

Figure 7. Transient absorption at 400 nm following radiolysis (42% of maximum dose) of mixtures of (A) 0.81, (B) 1.3, (C) 0.42 mbar NO_2, 5 mbar $C_4F_9OCH_3$, 25 mbar O_2, and 970 mbar SF_6 ($l = 120$ cm). Part D shows the transient absorption following radiolysis of a mixture of 0.76 mbar NO, 19 mbar $C_4F_9OCH_3$, 25 mbar O_2, and 970 mbar SF_6 ($l = 80$ cm). The smooth and dotted lines are simulations of the experimental transients; see text for details.

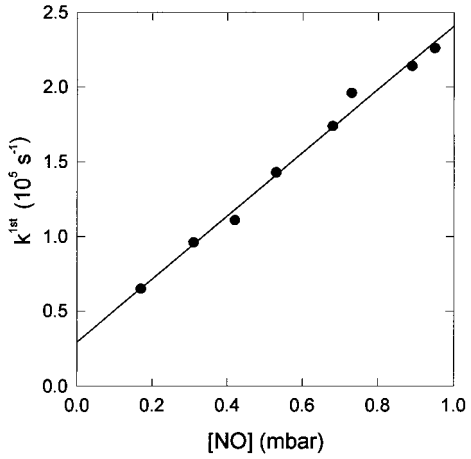

Figure 8. First order formation rates of NO_2 (formed from the reaction of NO with $C_4F_9OCH_2O_2$) observed following radiolysis of $SF_6/C_4F_9OCH_3/O_2$/NO mixtures as a function of NO concentration.

increase in absorption was fitted using the following expression for a first-order formation: $A(t) = (A_{inf} - A_0)(1 - \exp(-k^{first}t)) + A_0$, where $A(t)$ is the time dependent absorbance, A_0 is the extrapolated absorbance at time $t = 0$ (always close to zero), A_{inf} is the absorbance at infinite time, and k^{first} is the pseudo-first-order appearance rate of NO_2. This technique for measuring the rate constant for the reaction of NO with peroxy radicals is described in detail elsewhere.[21] Figure 8 shows a plot of k^{first} versus [NO]. Linear least-squares analysis of the data in Figure 8 gives $k_3 = (8.5 \pm 1.7) \times 10^{-12}$ cm^3 molecule^{-1} s^{-1}. The y-axis intercept is $(2.9 \pm 0.7) \times 10^4$ s^{-1} and suggests that the self-reaction of the $C_4F_9OCH_2O_2$ radicals contributes to the loss of $C_4F_9OCH_2O_2$ radicals. The decay half-life for the loss of $C_4F_9OCH_2O_2$ due to the self-reaction is approximately 28 μs at 42% of maximum dose. An intercept of 2.9×10^4 s^{-1} which is the same as a first order formation half-life for NO_2 of 34 μs is close to the decay half-life for $C_4F_9OCH_2O_2$ due to the self-reaction. Hence on a semiquantitative basis the intercept in Figure 8 can be explained by the self-reaction of $C_4F_9OCH_2O_2$

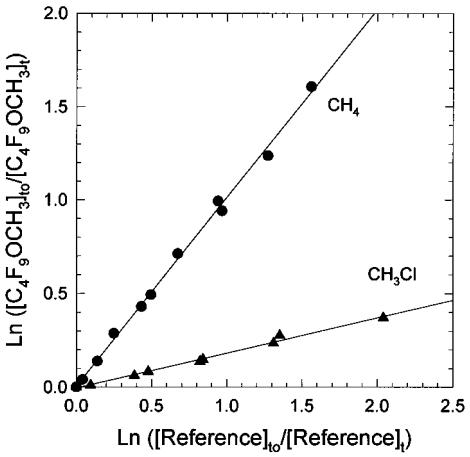

Figure 9. Decay of HFE-7100 versus CH_4 (triangles) and CH_3Cl (diamonds) in the presence of Cl atoms.

radicals. To test this hypothesis, the experimental transient shown in Figure 7D was simulated using a model consisting of the following reactions (and rate constants): F + RH (1.6×10^{-11}), R + O_2 (2.5×10^{-12}), R + R (3.5×10^{-11}), RO_2 + RO_2 (1.35×10^{-11}), RO_2 + NO (8.5×10^{-12}), RO + NO(1×10^{-11}), RO + NO_2 (1×10^{-11}), and RO_2 + NO_2 (8.8×10^{-12}) with $\sigma(NO_2) = 6.01 \times 10^{-19}$cm^2 molecule^{-1} at 400 nm.[15] The result is shown as the smooth curve in Figure 7D. The excellent fit of the model to the experimental data lends confidence to the value of $k_3 = (8.5 \pm 1.7) \times 10^{-12}$ cm^3 molecule^{-1} s^{-1} obtained here. We estimate that possible secondary chemistry contributes an additional 10% uncertainty to k_3. Hence we arrive at $k_3 = (8.5 \pm 2.5) \times 10^{-11}$ cm^3 molecule^{-1} s^{-1}.

3.10. Relative Rate Studies of the Reactions of Cl and F Atoms with HFE-7100. Prior to investigating the atmospheric fate of $C_4F_9OCH_2O\cdot$ radicals, relative rate experiments were performed using the FTIR system at Ford Motor Company to investigate the kinetics of reactions 13 and 14. The techniques used are described in detail elsewhere.[22] Photolysis of molecular halogen was used as a source of halogen atoms.

$$Cl_2 \text{ (or } F_2) + h\nu \rightarrow 2 \text{ Cl (or 2 F)} \quad (12)$$

$$Cl + C_4F_9OCH_3 \rightarrow C_4F_9OCH_2 + HCl \quad (13)$$

$$F + C_4F_9OCH_3 \rightarrow C_4F_9OCH_2 + HF \quad (14)$$

The kinetics of reaction 13 were measured relative to reactions 25 and 26. Reaction 14 was measured relative to reactions 27 and 28.

$$Cl + CH_4 \rightarrow \text{products} \quad (25)$$

$$Cl + CH_3Cl \rightarrow \text{products} \quad (26)$$

$$F + CH_4 \rightarrow CH_3 + HF \quad (27)$$

$$F + CD_4 \rightarrow CD_3 + DF \quad (28)$$

The observed losses of $C_4F_9OCH_3$ versus those of reference compounds in the presence of either Cl or F atoms are shown in Figures 9 and 10, respectively. The experiments described in this section were performed using a sample of HFE-7100 which consisted of 65% *i*-$C_4F_9OCH_3$ and 35% *n*-$C_4F_9OCH_3$. There was no discernible difference in reactivity (<5%) of Cl or F atoms toward the *i*- and *n*-isomers of HFE-7100. There was no discernible difference between data obtained in 700 Torr of either N_2 or air diluent. Linear least-squares analysis gives

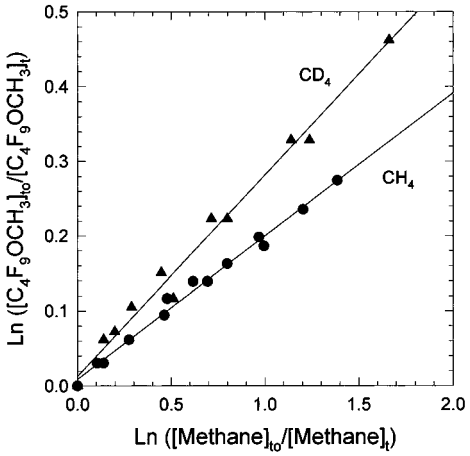

Figure 10. Decay of HFE-7100 versus CD_4 (circles) and CH_4 (diamonds) in the presence of F atoms.

$k_{13}/k_{25} = 1.00 \pm 0.05$, $k_{13}/k_{26} = 0.19 \pm 0.01$, $k_{14}/k_{27} = 0.19 \pm 0.01$, and $k_{14}/k_{28} = 0.27 \pm 0.02$. Using $k_{25} = 1.0 \times 10^{-13}$,[15] $k_{26} = 4.9 \times 10^{-13}$,[15] $k_{27} = 6.8 \times 10^{-11}$,[17] and $k_{28} = 4.7 \times 10^{-11}$,[17] the four ratios give $k_{13} = (1.00 \pm 0.05) \times 10^{-13}$, $k_{13} = (9.3 \pm 0.5) \times 10^{-14}$, $k_{14} = (1.3 \pm 0.1) \times 10^{-11}$, and $k_{14} = (1.3 \pm 0.1) \times 10^{-11}$ cm^3 molecule^{-1} s^{-1}, respectively. We estimate that potential systematic errors associated with uncertainties in the reference rate constants could add an additional 10% and 20% uncertainty ranges for k_{13} and k_{14}, respectively. Propagating these additional uncertainties gives values of $k_{13} = (1.00 \pm 0.11) \times 10^{-13}$, $k_{13} = (9.3 \pm 1.0) \times 10^{-14}$, $k_{14} = (1.3 \pm 0.3) \times 10^{-11}$, and $k_{14} = (1.3 \pm 0.3) \times 10^{-11}$ cm^3 molecule^{-1} s^{-1}. We choose to cite final values of k_{13} and k_{14}, which are averages of those determined using the two different reference compounds together with error limits which encompass the extremes of the individual determinations. Hence, $k_{13} = (9.7 \pm 1.4) \times 10^{-14}$ and $k_{14} = (1.3 \pm 0.3) \times 10^{-11}$ cm^3 molecule^{-1}s^{-1}. Quoted error reflects the accuracy of our measurements. The value of k_{14} determined using the FTIR technique is in agreement with the determination of $k_{14} = (1.6 \pm 0.6) \times 10^{-11}$ cm^3 molecule^{-1} s^{-1} using the pulse radiolysis technique (see section 3.4). There are no literature data available for k_{13} or k_{14} with which to compare our results.

3.11. Determination of the Atmospheric Fate of $C_4F_9OCH_2O^\bullet$ Radicals. The atmospheric fate of $C_4F_9OCH_2O$ radicals was studied using the FTIR−smog chamber system at Ford Motor Company.[7] Experiments were performed using the UV irradiation of $C_4F_9OCH_3/Cl_2/O_2/N_2$ mixtures with, and without, added NO. In these experiments, $C_4F_9OCH_2O$ radicals were formed either by reaction 18a or 3a.

$$C_4F_9OCH_2O_2 + C_4F_9OCH_2O_2 \rightarrow C_4F_9OCH_2O + C_4F_9OCH_2O + O_2 \quad (18a)$$

$$C_4F_9OCH_2O_2 + C_4F_9OCH_2O_2 \rightarrow C_4F_9OCHO + C_4F_9OCH_2OH + O_2 \quad (18b)$$

$$C_4F_9OCH_2O_2 + NO \rightarrow C_4F_9OCH_2O + NO_2 \quad (3a)$$

$$C_4F_9OCH_2O_2 + NO + M \rightarrow C_4F_9OCH_2ONO_2 + M \quad (3b)$$

Once formed, the $C_4F_9OCH_2O$ radicals are expected to undergo either reaction 22 or 29.

$$C_4F_9OCH_2O + O_2 \rightarrow C_4F_9OC(O)H + HO_2 \quad (22)$$

$$C_4F_9OCH_2O + M \rightarrow C_4F_9O + HCHO + M \quad (29)$$

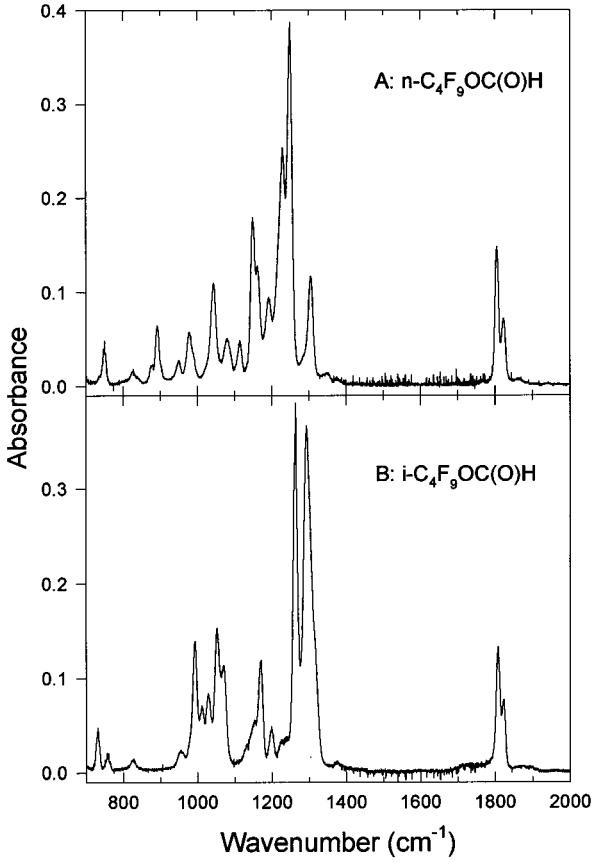

Figure 11. IR spectra of (A) 1.84 mTorr of *n*-$C_4F_9OC(O)H$ and (B) 1.88 mTorr of *i*-$C_4F_9OC(O)H$ derived from the Cl atom initiated oxidation of mixtures of either *n*-HFE-7100 (A) or *i*-HFE-7100 (B) in 700 Torr of air at 295 K.

Reaction 22 produces perfluorobutyl formate, while the unimolecular decomposition reaction 29 gives a perfluorobutyl alkoxy radical which will further decompose and initiate a sequence of reactions that "unzip" the radical. In the case of *n*-C_4F_9O, the reaction sequence 30−32 produces four molecules of COF_2, while for *i*-C_4F_9O radicals we expect the formation of two molecules of COF_2 and one of $CF_3C(O)F$.

$$C_nF_{2n+2}O + M \rightarrow C_{n-1}F_{2n} + COF_2 + M \quad (30)$$

$$C_{n-1}F_{2n} + O_2 \rightarrow C_{n-1}F_{2n}O_2 + M \quad (31)$$

$$C_{n-1}F_{2n}O_2 + NO \rightarrow C_{n-1}F_{2n}O + NO_2 \quad (32)$$

COF_2 is readily detectable by its absorption features at 774 and 1850−2000 cm^{-1} and serves as a convenient marker for the importance of reaction 29. The formation of perfluorobutyl formate serves as a marker for reaction 22. Four sets of experiments were performed with samples of *n*- and *i*-$C_4F_9OCH_3$ in the presence and absence of NO.

For small (1−10%) conversions of the HFE-7100 there was no detectable formation of COF_2 in the system, showing that reaction 29 is not an important loss mechanism of $C_4F_9OCH_2O$ radicals. IR product features were observed at 751, 827, 890, 976, 1041, 1080, 1113, 1149, 1192, 1230, 1249, 1304, 1805, and 1823 cm^{-1} in experiments employing *n*-HFE-7100 and 728, 825, 992, 1027, 1052, 1068, 1169, 1263, 1293, 1807, and 1822 cm^{-1} in experiments employing *i*-HFE-7100. As discussed below we ascribe these features to the perfluorobutyl formates and conclude that reaction 22 is the dominant loss of $C_4F_9OCH_2O$ radicals in the system. IR spectra of the formates are shown in Figure 11. Interestingly, there was no discernible

difference between the formate yields in experiments with, and without, added NO and no evidence for the formation of other carbon containing products. The only reasonable interpretation is that HFE-7100 is converted into formate in both systems in essentially 100% yield. On this basis we are able to calibrate the formate spectra shown in Figure 11. For Cl-atom-initiated oxidation experiments conducted in the absence of NO, we usually observe the formation of hydroperoxides via the reaction $RO_2 + HO_2 \rightarrow ROOH + O_2$ ($R = C_4F_9OCH_2$). The absence of hydroperoxides in the present experiments can be rationalized several ways: (i) the $RO_2 + HO_2$ reaction is unusually slow, (ii) the $RO_2 + HO_2$ reaction does not give ROOH but instead produces the formate (the analogous $CH_3OCH_2O_2 + HO_2$ reaction gives a substantial formate yield[23]), (iii) ROOH is formed in the system but is consumed by secondary reaction with Cl atoms to regenerate the peroxy radical, or (iv) a combination of the above.

Following the irradiation of HFE-7100/Cl_2/air mixtures, the concentration of the formates were observed to increase linearly with loss of HFE up until about 50% loss of the parent HFE-7100. For conversions of HFE-7100 > 85−90% the formate yield reached a plateau and then decreased. We ascribe this behavior to reaction of Cl atoms with the formate. By monitoring the formation and subsequent loss of the formate as a function of the fractional conversion of HFE-7100, we can establish the rate constant for reaction of Cl atoms with the formates.

$$Cl + C_4F_9OC(O)H \rightarrow HCl + C_4F_9OC(O) \qquad (33)$$

The relevant reactions are 33 and 34

$$Cl + \text{HFE-7100} \rightarrow \alpha \text{ formate} + \text{other products} \qquad (34)$$

where α is the yield of formate from HFE-7100 ($0 < \alpha < 1$). The corresponding rate equations can be solved analytically to relate the amount of formate at any time t to the corresponding conversion of HFE-7100 at time t as a function of α and the rate constant ratio k_{33}/k_{34}, where k_{33} and k_{34} are the bimolecular rate constants of reactions 33 and 34, respectively. The expression, as derived in reference 24, is

$$\frac{[\text{formate}]_t}{[\text{HFE-7100}]_{t_0}} = \frac{\alpha}{1 - \frac{k_{33}}{k_{34}}}(1 - x)[(1 - x)^{\{k_{33}/k_{34} - 1\}} - 1] \qquad (I)$$

where x is the conversion of HFE-7100, defined as

$$x \equiv 1 - \frac{[\text{HFE-7100}]_t}{[\text{HFE-7100}]_{t_0}}$$

Figure 12 shows plots of the observed concentration of $C_4F_9OC(O)H$ normalized to the initial HFE-7100 concentration versus the fractional loss of HFE-7100 following irradiations of mixtures of HFE-7100 and Cl_2 in 700 Torr of air diluent. Fits of expression I to the data in Figure 12A,B give values of $k_{33}/k_{34} = 0.20 \pm 0.04$ and 0.14 ± 0.05 for the *n*- and *i*-isomers, respectively. Within the experimental uncertainties there is no significant difference in reactivity of the two formate isomers with Cl atoms, and we choose to quote an average value of $k_{33}/k_{34} = 0.17 \pm 0.07$ with error limits that encompass the extremes of the individual determinations. Using k(Cl+HFE-7100) = $(9.7 \pm 1.4) \times 10^{-13}$, we arrive at $k_{33} = (1.6 \pm 0.7) \times 10^{-14}$ cm^3 molecule^{-1} s^{-1}.

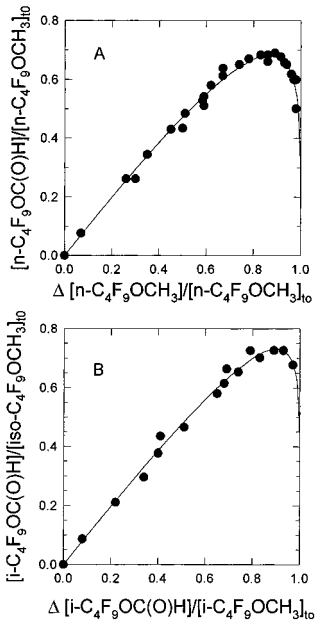

Figure 12. Plots of the observed concentration of $C_4F_9OC(O)H$ normalized to the initial HFE-7100 concentration versus the fractional loss of HFE-7100 following irradiations of mixtures of HFE-7100 and Cl_2 in 700 Torr of air diluent. Part A shows the data for the *n*-isomer while panel B shows data for the *i*-isomer. The curves are fits to the data; see text for details.

For completeness the Cl-atom-initated oxidation of the formates was studied as part of the present work. The experimental method was as follows. Mixtures of 4−5 mTorr of either *n*-HFE-7100 or *i*-HFE-7100, 200−300 mTorr of Cl_2, 16−18 mTorr of NO, and 40 Torr of O_2 in 50 Torr total pressure of N_2 diluent were prepared and irradiated for successive 2 min periods until all IR features attributed to the HFE-7100 had disappeared. The product mixtures were then subject to further UV irradiation, and the loss of formate and formation of COF_2 and $CF_3C(O)F$ were monitored. The results are shown in Figure 13. The radical formed in reaction 33 is expected to add O_2, react with NO to give the corresponding alkoxy radical, and then decompose to give a perflurobutyl alkoxy radical which will "unzip" via reactions 30−32. As expected, the oxidation of *n*-$C_4F_9OC(O)H$ gave a molar COF_2 yield of 370 ± 63% while *i*-$C_4F_9OC(O)H$ degradation gave molar yields of 172 ± 30% COF_2 and 101 ± 18% $CF_3C(O)F$. Quoted errors include two standard deviations from linear regressions of the data in Figure 13 plus an additional 15% uncertainty associated with uncertainties in the calibrations of the COF_2, $CF_3C(O)F$, and formate reference spectra.

3.12. Computational Study of Perfluoroalkyl Formate IR Spectra. A surprising feature of the perfluoroalkyl formate vibrational is the presence of *two* bands in the carbonyl stretch region. Ab initio calculations were performed to examine the vibrational spectra of the formates, using $CF_3OC(O)H$ as a simple model for the higher homologues. Alkyl formates can exist in both syn and anti conformers. If R is a hydrocarbon,

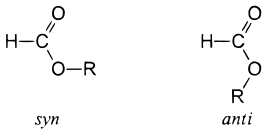

the syn conformer is preferred to the anti by several kcal mol^{-1}, the barrier for interconversion is approximately 10 kcal mol^{-1},

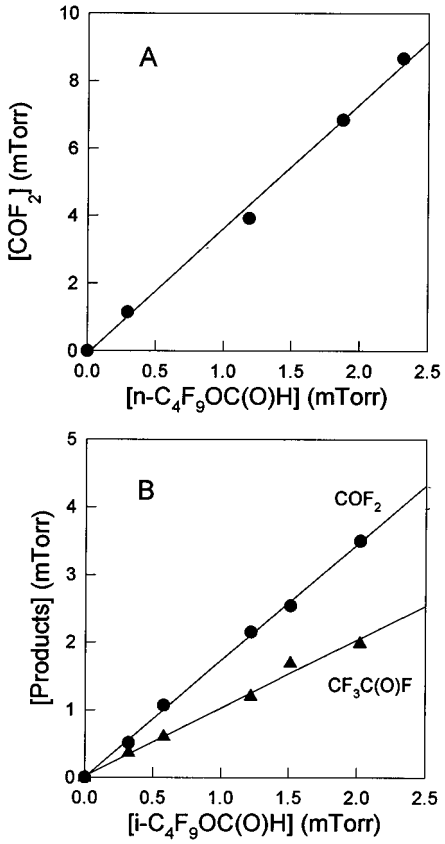

Figure 13. Product yields following the Cl atom initiated oxidation of (A) *n*-$C_4F_9OC(O)H$ and (B) *i*-$C_4F_9OC(O)H$; see text for details.

and only the syn is observed under normal conditions.[25] If R = CF_3, however, we find that the two conformers are much closer in energy, and that the rotational barrier separating the two decreases. Such differences are consistent with the strong π-accepting influence of the CF_3 group.[26]

Table 3 contains the results of ab initio calculations on the two conformers and the transition state connecting them. The two differ only slightly in structure, and at the highest level of theory considered, the syn is more stable than the anti by only 1.2 kcal mol^{-1}. Zero-point energy and thermal effects decrease this difference to about 1 kcal mol^{-1}, which implies a relative population of approximately 80% syn to 20% anti at 298 K. The barrier separating these two is approximately 7 kcal mol^{-1}. Assuming a prefactor of about 10^{12} s^{-1}, the conformer lifetime is roughly 0.1 μs, sufficient for the two conformers to be resolved in infrared experiments. Harmonic vibrational frequencies were calculated for both conformers, and the frequencies scaled by 0.873 to facilitate comparison with experiment (scale factor determined by comparison of the experimental and calculated spectra of methyl formate). The calculated carbonyl stretch bands for the two conformers are in excellent agreement with the two bands observed in both *n*- and *i*-$C_4F_9OC(O)H$, and we assign the low-and high-energy bands to the syn and anti conformers, respectively. When weighted by the relative populations of the two conformers (Table 3), the calculated intensities of the two bands are in excellent agreement with experiment. A number of other vibrational doublets are expected for the two conformers, but the most prominent are likely obscured by the large number of intense C−F stretch bands from the perfluorobutyl chains.

4.0. Implications for Atmospheric Chemistry

We present herein a large body of kinetic and mechanistic data pertaining to the atmospheric chemistry of HFE-7100. The atmospheric lifetime of HFE-7100 is determined by its reaction with OH radicals and is estimated to be ≈5 years. Reaction with OH gives the alkyl radical $C_4F_9OCH_2$ which, within less than 1 μs, will be converted into the corresponding peroxy radical $C_4F_9OCH_2O_2$. We show here that $C_4F_9OCH_2O_2$ radicals react rapidly with NO to produce NO_2 and, by inference $C_4F_9OCH_2O$ radicals. Using $k_3 = 8.5 \times 10^{-12}$ cm^3 $molecule^{-1}$ s^{-1} together with an estimated background tropospheric NO concentration of 2.5×10^8 molecule cm^{-3}, the lifetime of $C_4F_9OCH_2O_2$ radicals with respect to reaction with NO is calculated to 8 min. Reaction 3 is likely to be an important atmospheric loss of $C_4F_9OCH_2O_2$ radicals. The sole fate of the alkoxy radical derived from HFE-7100 is reaction with O_2 to give the formate. This behavior is entirely consistent with the available database concerning the behavior of similar nonfluorinated alkoxy radicals, e.g., CH_3OCH_2O and $(CH_3)_3COCH_2O$ radicals are known to exclusively react with O_2 to give formates.[27] It is reported herein that the formate $C_4F_9OC(O)H$ is rather unreactive toward Cl atoms and is likely to be similarly unreactive toward OH radicals. Organic compounds which react with Cl atoms with rate constants in the range $10^{-14}-10^{-13}$ cm^3 $molecule^{-1}$ s^{-1} generally react faster with Cl atoms than with OH radicals.[15] Hence, we can use the value of $k_{33} = 1.6 \times 10^{-14}$ cm^3 $molecule^{-1}$ s^{-1} as an upper limit to k(OH+$C_4F_9OC(O)H$). Using a 24 h global average OH concentration of 7.5×10^5 cm^{-3}, we derive a lower limit of 3 years for the atmospheric lifetime of $C_4F_9OC(O)H$ with respect to reaction with OH radicals. In view of the polar nature of $C_4F_9OC(O)H$ it seems likely that the main atmospheric removal mechanism of this compound will be via wet/dry deposition and possibly photolysis. Unfortunately, there are no available data for the rates of these processes and hence it is not possible to provide an estimate of the atmospheric lifetime of $C_4F_9OC(O)H$ at this time.

TABLE 3: Selected Geometry Parameters, Vibrational Frequencies and Intensities, Dipole Moments, and Relative Energies of Stable $CF_3OC(O)H$ Conformers and Transition State Connecting Them

	syn-$CF_3OC(O)H$	TS	*anti*-$CF_3OC(O)H$
Selected Geometric Parambers[a]			
C_H=O	1.203	1.198	1.200
C_H−O	1.386	1.417	1.395
C_F−O	1.384	1.361	1.371
H−C_H	1.091	1.091	1.093
F−C_F	1.333, 1.337	1.330, 1.343, 1.353	1.327, 1.346
∠O=C_H−O	126.0	122.5	120.4
∠H−C_H−O	107.0	110.9	113.2
∠C_H−O−C_F	117.5	115.7	115.9
∠O=C_H−O−C_F	0	92.3	180
Selected Vibrational Frequencies and Intensities[b]			
ν(C_H−H)	2895 (5)		2874 (1)
ν(C_H=O)	1800 (55)		1823 (13)
ν(H−C_H−O)	1351 (3)		1377 (1)
ν(F−C_F)	1284 (66)		1309 (23)
ν(F−C_F)	1260 (62)		1250 (22)
ν(C_F−O)	1199 (100)		1224 (16)
ν(C_O−O)	1129 (32)		1086 (9)
Dipole Moments[c]			
	1.91	1.86	1.80
Relative Energies[d]			
RHF/6-31G(d,p)	0	7.8	2.2
MP2/6-31G(d,p)	0	8.2	2.1
MP2/TZ2P	0	7.5	1.2
ZPE[e]	0	−0.6	−0.2

[a] MP2/6-31G(d,p) distances in angstroms, angles in degrees. [b] RHF/6-31G(d,p) frequencies in cm^{-1}, scaled by 0.873. RHF/6-31G(d,p) intensities weighted by relative thermal populations at 298 K and normalized to 100 maximum. [c] MP2/6-31G(d,p), in debye. [d] In kcal mol^{-1}. [e] Zero-point energy, from unscaled frequencies.

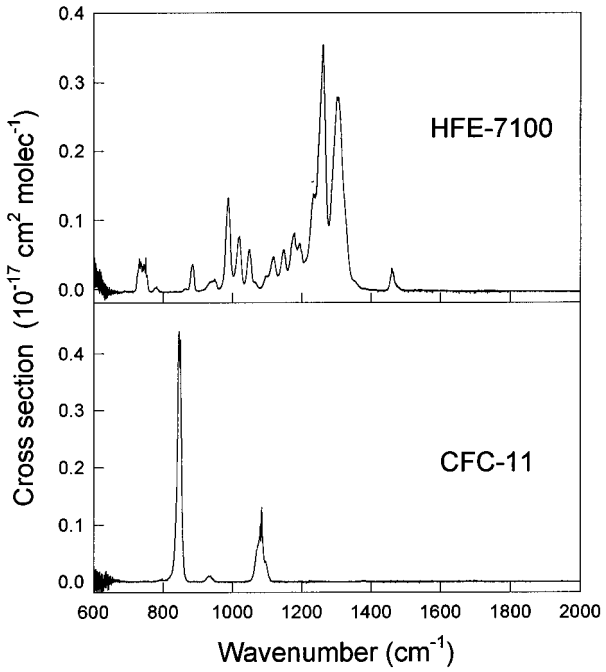

Figure 14. IR spectra of HFE-7100 (mixture of *n*- and *i*-isomers used commercially) and CFC-11.

The atmospheric degradation of HFEs produce the same fluorinated radical species as formed during the degradation of HFCs. HFCs do not impact stratospheric ozone,[4] and the same conclusion applies to HFEs. HFE-7100 has an ozone depletion potential of zero. Finally we need to consider the potential for HFE-7100 to impact the radiative balance in the atmosphere. Using the method of Pinnock et al.[28] with the IR spectra shown in Figure 14 we calculate instantaneous forcings for HFE-7100 and CFC-11 of 0.37 and 0.26 W/m^2, respectively. Values of the GWP (global warming potential) for HFE-7100 (relative to CFC-11) can then be estimated using the expression[29]

$$GWP_{\mathrm{HFE-7100}} = \left(\frac{\mathrm{IF_{HFE-7100}}}{\mathrm{IF_{CFC-11}}}\right)\left(\frac{\tau_{\mathrm{HFE-7100}}M_{\mathrm{CFC-11}}}{\tau_{\mathrm{CFC-11}}M_{\mathrm{HFE-7100}}}\right)\left(\frac{1-\exp(-t/\tau_{\mathrm{HFE-7100}})}{1-\exp(-t/\tau_{\mathrm{CFC-11}})}\right)$$

where $\mathrm{IF_{HFE-7100}}$, $\mathrm{IF_{CFC-11}}$, $M_{\mathrm{HFE-7100}}$, $M_{\mathrm{CFC-11}}$, $\tau_{\mathrm{HFE-7100}}$, and $\tau_{\mathrm{CFC-11}}$ are the instantaneous forcings, molecular weights, and atmospheric lifetimes of the two species and t is the time horizon over which the forcing is integrated. Using $\tau_{\mathrm{HFE-7100}} \approx 5$ years and $\tau_{\mathrm{CFC-11}} = 50$ years,[28] we estimate that the GWP of HFE-7100 is ≈0.23 for a 20 year horizon and ≈0.091 for a 100 year time horizon. The GWP of HFE-7100 is a factor of 5−20 less than those of the CFCs that it replaces.

Acknowledgment. We thank Fred Behr (3M Corp.) for supplying samples of HFE-7100 and Robert Meagher and Mark McIntosh for their help in conducting experiments at Ford. The work at Risø was supported by the European Union.

References and Notes

(1) Molina, M. J.; Rowland, F. S. *Nature* **1974**, *249*, 810.

(2) Farman, J. D.; Gardiner, B. G.; Shanklin, J. D. *Nature* **1985**, *315*, 207.

(3) Product information sheet from 3M Specialty Chemicals Division, **1996**.

(4) Wallington, T. J.; Schneider, W. F.; Worsnop, D. R.; Nielsen, O. J.; Sehested J.; Debruyn, W. J.; Shorter, J. A. *Environ. Sci. Technol.* **1994**, *28*, 320.

(5) Tang, Y. *Atmospheric Fate of Various Fluorocarbons*, MS Thesis, Massachusetts Institute of Technology, 1993.

(6) Hansen, K. B.; Wilbrandt, R., Pagsberg, P. *Rev. Sci. Instrum.* **1979**, *50*, 1532.

(7) Wallington, T. J.; Japar, S. M. *J. Atmos. Chem.* **1989**, *9*, 399.

(8) Bilde, M.; Møgelberg, T. E.; Sehested, J.; Nielsen, O. J., Wallington, T. J.; Hurley, M. D.; Japar, S. M.; Dill, M.; Orkin, V. L.; Buckley, T. J.; Huie, R. E.; Kurylo, M. J. *J. Phys. Chem. A* **1997**, *101*, 3514.

(9) Wallington, T. J.; Dagaut, P.; Kurylo, M. J. *Chem. Rev.* **1992**, *92*, 667.

(10) Schmidt, M. W.; Baldridge, K. K.; Boatz, J. A.; Elbert, S. T.; Gordon, M. S.; Jensen, J. H.; Koseki, S.; Matsunaga, N.; Nguyen, K. A.; Su, S. J.; Windus, T. L.; Dupuis, M.; Montgomery, J. A. *J. Comput. Chem.* **1993**, *14*, 1347.

(11) Stanton, J. F.; Gauss, J.; Watts, J. D.; Lauderdale, W. J.; Bartlett, R. J. ACES II (an ab initio program system); Quantum Theory Project, University of Florida, Gainesville.

(12) Hariharan, P. C.; Pople, J. A., *Theor. Chim. Acta* **1973**, *28*, 213.

(13) Bartlett, R. J. *Annu. Rev. Phys. Chem.* **1981**, *32*, 359.

(14) Pople, J. A.; Krishnan, R.; Schlegel, H. B.; Binkley, J. S. *Int. J. Quantum Chem. Symp., Quantum Chem.* **1979**, *13*, 1325.

(15) DeMore, W. B.; Sander, S. P.; Golden, D. M.; Hampson, R. F.; Kurylo, M. J.; Howard, C. J.; Ravishankara, A. R.; Kolb, C. E.; Molina, M. J.; JPL Publication No. 94-26; NASA Jet Propulsion Laboratory: Pasadena, CA, 1994.

(16) Prinn, R. G.; Weiss, R. F.; Miller, B. R.; Huang, J.; Alyea, F. N.; Cunnold, D. M.; Fraser, P. J.; Hartley, D. E.; Simmonds, P. G. *Science* **1995**, *269*, 187.

(17) Wallington, T. J.; Hurley, M. D.; Maricq, M. M.; Sehested, J.; Nielsen, O. J.; Ellermann, T. *Int. J. Chem. Kinet.* **1993**, *25*, 651.

(18) Ellermann, T.; Sehested, J.; Nielsen, O. J.; Pagsberg, P.; Wallington, T. J. *Chem. Phys. Lett.* **1994**, *218*, 287.

(19) Lightfoot, P. D.; Cox, R. A.; Crowley, J. N.; Destriau, M.; Hayman, G. D.; Jenkin, M. E.; Moortgat, G. K.; Zabel, F. *Atmos. Environ.* **1992**, *26A*, 1805.

(20) Bjergbakke, E., Sehested, K; Rasmussen, O. L.; Christensen, H. **1984**, Risø-M-2430; RisøNational Laboratory: Roskilde, Denmark, 1984.

(21) Sehested, J.; Nielsen, O. J.; Wallington, T. J. *Chem. Phys. Lett.* **1993**, *213*, 457.

(22) Wallington, T. J.; Hurley, M. D. *Chem. Phys. Lett.*, **1992**, *189*, 437.

(23) Wallington, T. J.; Hurley, M. D.; Ball, J. C.; Jenkin, M. E. *Chem. Phys. Lett.* **1993**, *211*, 41.

(24) Meagher, R. J.; McIntosh, M. E.; Hurley, M. D.; Wallington, T. J. *Int. J. Chem. Kinet.* **1997**, *29*, 619.

(25) (a) Blom, C. E.; Günthard, Hs. H. *Chem. Phys. Lett.* **1981**, *84*, 267. (b) Choi, P.-K.; Naito, Y.; Takagi, K. *Chem. Phys. Lett.* **1985**, *121*, 169. (c) Bond, D.; Schleyer, P. v. R. *J. Org. Chem.* **1990**, *55*, 1003 and references therein.

(26) Schneider, W. F.; Nance, B. I.; Wallington, T. J. *J. Am. Chem. Soc.* **1995**, *117*, 478.

(27) Japar, S. M.; Wallington, T. J.; Richert, J. F. O.; Ball. J. C. *Int. J. Chem. Kinet.* **1990**, *22*, 1257.

(28) Pinnock, S.; Hurley, M. D.; Shine, K. P.; Wallington, T. J.; Smyth, T. J. *J. Geophys. Res.* **1995**, *100*, 23227.

(29) Houghton, J. T.; Meira Filho, L. G.; Bruce, J.; Lee, H.; Callander, B. A.; Haites, E.; Harris, N.; Maskell, K. *Climate Change 1994: Radiative Forcing of Climate Change and an evaluation of the IPCC IS92 Emission Scenarios*; Houghton, J. T., Ed.; Cambridge University Press: Cambridge, 1995; p 222 (Report of Working Groups I and III of the Intergovernmental Panel on Climate Change).